



### **Science Arts & Métiers (SAM)**

is an open access repository that collects the work of Arts et Métiers Institute of Technology researchers and makes it freely available over the web where possible.

This is an author-deposited version published in: <https://sam.ensam.eu>  
Handle ID: <http://hdl.handle.net/10985/24792>

#### **To cite this version :**

M. PRANIEWICZ, Lucas FOURNET-FAYARD, J.C. FOX, C. CAYRON, Imade KOUTIRI, Anne-Françoise OBATON - Bearing area curve based partitioning for the verification of theoretical supplemental geometry on additively manufactured lattice structures - Additive Manufacturing - 2023

Any correspondence concerning this service should be sent to the repository

Administrator : [scienceouverte@ensam.eu](mailto:scienceouverte@ensam.eu)



# Bearing area curve based partitioning for the verification of theoretical supplemental geometry on additively manufactured lattice structures

M. Pranievicz<sup>a,\*</sup>, L. Fournet-Fayard<sup>b</sup>, J.C. Fox<sup>a</sup>, C. Cayron<sup>b</sup>, I. Koutiri<sup>c</sup>, A.-F. Obaton<sup>b</sup>

<sup>a</sup> National Institute of Standards and Technology,<sup>1</sup> Gaithersburg, MD 20899, USA

<sup>b</sup> Laboratoire Commun de Métrologie (LCM), Laboratoire National de Métrologie et d'Essais (LNE), 75015 Paris, France

<sup>c</sup> Laboratoire PIMM, Arts et Métiers Institute of Technology, CNRS, Cnam, HESAM University, 75013 Paris, France

## ARTICLE INFO

### Keywords:

Lattice Structures  
Additive Manufacturing  
Qualification  
Form Measurement  
Theoretical Supplemental Surface

## ABSTRACT

The geometrical qualification of additively manufactured lattice structures has largely focused on the measurement of strut diameter, form variations, and surface texture. However, the exterior surfaces of the lattice structure, defined through theoretical supplemental geometry, are critical surfaces that dictate the contact area of the structure on other components within assemblies. Form variations on these surfaces complicate the measurement process by adding ambiguity into what surfaces of the component belong to the controlled geometry. Previous works have developed novel methods to improve data extraction for the measurement of these surfaces using computer aided design (CAD) data for various lattice structures. This work presents an adaptation of these methods to work with additively manufactured (AM) geometries, specifically designing the methodology to account for the form variations between lattice struts. The presented results show the applicability of these methods to AM lattice structures for the measurement of form defined by a theoretical supplemental surface.

## 1. Introduction

Additive manufacturing (AM) has matured beyond the laboratory and into industrial production. Manufacturers are now incorporating components produced via AM into consumer products. The design freedom afforded through the AM process allows for the creation of complex geometries that otherwise would not be possible through more conventional manufacturing processes. A prime example of the complexities enabled by AM are lattice structures, defined as a “geometric arrangement composed of connective links between vertices (points) creating a functional structure” [1]. These structures are often designed by patterning an array of a designed unit cell [2]. The dimensions of this unit cell can even be modified throughout the volume of a component to maximize the strength to weight ratio [3]. Applications of these structures include biomedical implants to improve bone integration, weight reduction in structural components, energy absorbing structures, catalysts, and heat exchangers [4].

While the nominal design of these structures can be tuned dramatically to improve mechanical or thermal properties, geometric errors in

the as-built components often hinder their performance. Thus, researchers have sought to understand how these geometrical imperfections, which occur on several different length scales, impact the mechanical properties of these structures. Often, this involves utilizing X-ray computed tomography (XCT) to measure an AM lattice structure. The XCT measurement process generates a full volumetric model of a scanned object, allowing access to features often not measurable by other techniques [5]. The measurement results from XCT can then be imported into a finite-element modeling software to simulate mechanical testing [6]. XCT measurements have also been used to estimate and model fatigue behavior in AM lattice structures [7]. Other researchers have sought to simulate these geometric imperfections, rather than relying on XCT measurements, which are often limited in accuracy and repeatability [8]. While XCT has the capability of providing rich geometric information, it is not capable of achieving traceable measurements of a geometrically complex lattice structure. This traceability is often a requirement for the establishment of quality management systems and therefore the qualification of components [9]. However, it has commonly been used for comparison measurements, and research

\* Corresponding author.

E-mail address: [maxwell.praniewicz@nist.gov](mailto:maxwell.praniewicz@nist.gov) (M. Pranievicz).

<sup>1</sup> Certain commercial entities, equipment, or materials may be identified in this document to describe an experimental procedure or concept adequately. Such identification is not intended to imply recommendation or endorsement by the National Institute of Standards and Technology, nor is it intended to imply that the entities, materials, or equipment are necessarily the best available for the purpose.

continues on developing traceable measurement techniques for internal or geometrically complex features [10,11]. Because of this, the measurement of lattice structures using XCT is often paired with other measurement techniques for comparison [12]. Several recent works have taken initial steps toward providing traceable XCT measurements of lattice struts [13,14].

While strut geometry is the most common inspection criteria in the literature, the exterior surfaces which define the boundaries of a lattice structure also play a critical role in the function of a lattice component. These surfaces dictate the mechanical contact of the component with mating surfaces, leading to changes in the transfer of loads or conductive heat transfer. A prime example of this is in compression applications, where the struts of the lattice are used as the load bearing area [15]. If form variations occur on these surfaces, the failure initialization zones within the lattice could shift unpredictably. Tools outlined in ASME Y14.46 2022 can be used to assign geometric controls of these surfaces to specify acceptable limits of form variation [16]. A theoretical supplemental surface (TSS), defined in ASME Y14.46 as “supplemental geometry, explicitly defined in the design model and similar to true profile, that may be used to control the form, size, orientation, or location of a functional collection of points, lines, surfaces, or any combination thereof” can be used to control the form of individual surfaces [17,18]. Investigations on the qualification of TSS or theoretical supplemental geometry (TSG) defined surfaces have indicated difficulty in the extraction of data from the defined surfaces due to ambiguity in discerning the boundary between the exterior, meaning the surface of the lattice intersecting and controlled by TSG, and interior, meaning the remainder of the lattice volume contained within the TSG, of a manufactured lattice [19,20]. This operation is analogous to partitioning, defined in ISO 17450-1: 2011 as a “feature operation used to identify a portion of a geometrical feature belonging to the real surface of the workpiece or to a surface model of the workpiece” [21]. Because of these complexities, recent works have utilized techniques borrowed from surface metrology to identify or partition data for the extraction of features. The Bearing Area (BA) curve, formally known as the Abbott-Firestone curve, has been traditionally used to define functional parameters in surface metrology [22]. However, it has been recently adapted to characterize open pores on AM surfaces and to examine the effect of process parameters on the surface texture and spatter [23,24].

The inspection of features defined by TSG is often a non-trivial task, as it is unclear where the boundary between the exterior and the interior of a lattice structure lies due to form variations and small feature sizes, as shown in Ref [20]. Thus, it is unclear where to extract data for feature association and analysis. Praniewicz et al. proposed a methodology to calculate the boundary of the interior and exterior of a lattice structure using BA curve to calculate a segmentation point along an evaluation direction, thus removing the ambiguity in the extraction process [25]. This segmentation point, redefined as the partition point in this work to be more consistent with geometric product definition standards, defines the boundary between the interior and exterior of the lattice structure. Previously demonstrated BA methodologies to extract data from lattice structures for the inspection of a TSS may not be well suited for lattice structures where individual struts comprise a theoretical surface, as opposed to one continuous surface formed by the intersection of several lattice unit cells. Because of manufacturing inconsistencies, the individual struts will likely vary in geometry. This would therefore affect the total region of interest required for these previously defined BA extraction methods. Thus, when the partitioning is performed on all surfaces at once, the calculated partition point may lie above the entirety of a shorter strut. Thus, it is more apt to perform individual BA partitioning calculations for each independent surface of the feature, in this case on the individual struts, and compile the data for feature analysis to inspect a TSS.

In this work, a metallic lattice structure is produced using Laser Powder bed Fusion (L-PBF) AM. The lattice structure is investigated using a BA curve automated partitioning methodology to assess the form

on an area defined by a TSS. A lattice structure is first designed and manufactured using AM. The component is then scanned using XCT and the determined surface is exported. A new BA partitioning methodology is presented to investigate the AM component. This novel methodology includes the integration of strut separation and partitioning of individual struts using an adaptive partitioning method which automatically determines the partitioning methodology based on the bearing area curve. Results of the strut partitioning processes are presented along with the measured form. These results convey the need for the unique adaptations to the BA curve methodology in the measurement of AM components.

## 2. Methodology

The unit cell chosen for the lattice structure investigated in this work was a cubic cell with a strut length of 2 mm and thickness of 0.3 mm, as seen in Fig. 1(a). The unit cell was replicated 10 times in each direction to obtain the overall lattice structure, shown as the computer aided design (CAD) model in Fig. 1(b). A substrate was built underneath the lattice, shown in Fig. 1(b) and (c), to aid in the registration of the component for further measurement and separation from the build plate. The cubic unit cell type has been chosen as it is relatively simple to characterize and will provide several individual surfaces defined by one TSS.

The lattice structure was manufactured on a 3DSystems ProX DMP320 L-PBF machine, equipped with a polymer scraper and an ytterbium fiber laser, which had a measured spot diameter of 70  $\mu\text{m}$ . The powder used in the AM system was Inconel 625 and had a size distribution centered around 32  $\mu\text{m}$ . The scanning strategy was defined by a single contour step, a filling step with a hatch of 85  $\mu\text{m}$ , and a rotation of 65° between each layer. Concerning the process parameters applied for the part, a laser power of 250 W and a scanning speed of 1 m/s were chosen for the filling step, while the contour step had a laser power of 180 W and a scanning speed of 1.900 m/s. The layer thickness was set to 60  $\mu\text{m}$ . Supports were positioned under the substrate to help the removal of the structure from the build platform.

The lattice structure was scanned by a METROTOM X-ray computed tomography (XCT) system by Carl Zeiss France (Fig. 2). The XCT parameters and the voxel size are given in the Table 1.

The data was then processed within VGStudio Max. The air/material boundary surface of the lattice structure was initially determined from the histogram, and then refined after the removal of the lattice substrate in the software, in order to obtain a better match between the iso-surface and the XCT scan. The file was afterwards converted to a stereolithography (STL) file with a resolution of 30.12  $\mu\text{m}$  (Fig. 3).

To reduce the total computational effort and limit the data to a smaller sample which can be presented with greater detail in this work, a section from the top surface along the build direction of the lattice was sectioned to yield a  $3 \times 3$  array of lattice struts for inspection, shown in Fig. 4. This subsection of the upward facing struts was chosen at random from the upward facing struts as a small representation of the average build geometry. This subsection of the lattice was evaluated for flatness using a theoretical supplemental surface, as shown in Fig. 4. It is worth noting that the struts in this lattice were designed to have a square cross

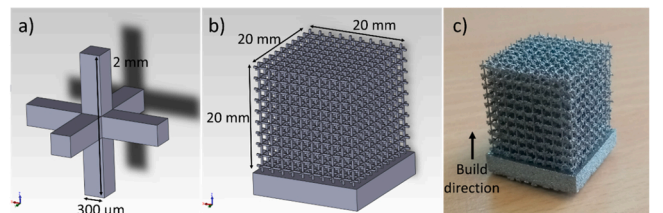


Fig. 1. Illustration of (a) CAD design of the lattice cell, (b) CAD design of the full lattice structure, (c) manufactured lattice structure.

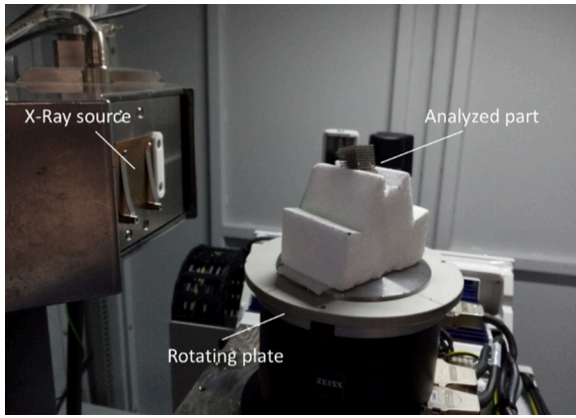


Fig. 2. Positioning of the sample in the XCT chamber.

**Table 1**  
XCT measurement parameters.

Parameter	Value
Voltage	200 kV
Current	135 $\mu$ A
Number of Projections	900
Images Averaged Per Projection	2
Integration Time	2 s
Detector Pixel Pitch	200 $\mu$ m
Geometric Magnification	6.64
Voxel Size (VS)	30.12 $\mu$ m x 30.12 $\mu$ m x 30.12 $\mu$ m
Physical Filter	2.0 mm Cu

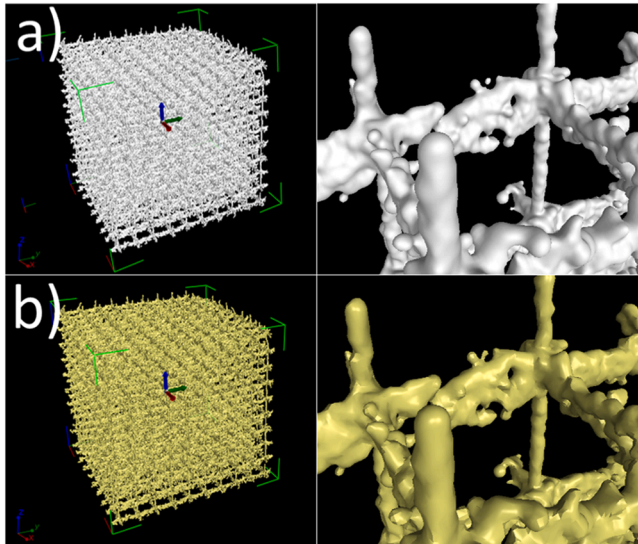


Fig. 3. Representation of the lattice structure as (a) XCT scan after iso-surface determination; (b) STL converted file.

section and flat external surfaces. Examining Figs. 3 and 4 shows that the AM process had difficulty in creating these geometries.

### 3. Theory/calculations

After the data was initially processed, it was imported into MATLAB as a mesh defined as a list of vertices,  $V$ , and faces that utilize such vertices,  $F$ , for evaluation using the BA partitioning described below. First, the evaluation orientation was selected as progressing along the -Z direction of the lattice. The evaluation limits of the lattice were then

defined by inputting the extremes of the lattice in the two directions orthogonal to the analysis direction and the limits of height to be investigated on the lattice. The limits along the evaluation orientation were set to 19.20 – 18.75 mm. These values were set such that the upper limit was above the tallest strut investigated. The lower limit was set such that the top surfaces of the lowest strut were included in the evaluation window. It is important to note that the lower limit of the investigation volume has an effect on the measurement result and users should report these limits to ensure an unambiguous measurement process. An example of the investigation volume is shown as the rectangular cuboid in Fig. 5. Other inputs included in this stage were the evaluation window thickness,  $w$ , and the grid spacing,  $d$ . The complete definitions for these terms can be found in [25].

The areas of the lattice structure that lie within the investigation volume are sectioned from the lattice structure. If a mesh element crossed the boundary of the investigation volume, it was split and only the area within the investigation volume was retained. This new mesh was defined by vertices  $V_{seg}$  and faces  $F_{seg}$ . Since, in these lattice structures, the individual struts can vary significantly in length, the BA partitioning should be performed individually on a strut-by-strut basis. The data from the individually extracted struts can then be analyzed together to determine the form of the defined geometry. Thus, the struts were segmented into their own individual mesh data sets. This was completed by importing  $V_{seg}$  into a point cloud segmentation algorithm within MATLAB (pcsegdist) which separates a point cloud into clusters based on Euclidean distance using a threshold of 0.25 mm. The separated point clouds for a given strut,  $V_{seg,i}$ , were then matched with their corresponding faces of  $F_{seg}$  to form the faces of a given strut,  $F_{seg,i}$ . The separate struts could then be processed individually using the BA methodology. The individually sectioned struts with labels can be seen in Fig. 5.

The BA curve generation for each individual strut was then completed similar to that in Ref [25]. The evaluation window of thickness  $w$  was then translated along the selected orientation in steps of  $w$ . For each step, the surface area of the mesh contained within the window was saved as an individual mesh data set. These surfaces could be used to construct the BA curve. However, surface areas under overhanging structures or unexposed triangles of the mesh could be captured in this process and do not accurately represent the actual bearing area of the surface. Therefore, the mesh was discretized using the following method.

A grid of points was created at the maximum extent of the evaluation direction in a plane normal to the evaluation orientation and arrayed along two mutually orthogonal directions with an even grid spacing of  $d$ . This array of points is shown in red in Fig. 6. Each point in this array was then projected along the evaluation orientation on the mesh area captured in the previous step and the intersection point was determined. If the projected point intersected the mesh area more than once, the first point along the projection path was used, eliminating the capture of overhanging surfaces. Material in overhangs or re-entrant material is not on the exterior of the component, as there is other material surrounding them. Therefore, surface data in these scenarios are not considered in the calculation of the partition point for the evaluation of form on the exterior of the lattice. The mesh element the point intersected, and its corresponding height recorded in the mesh area captured, were recorded. These projected points can be seen as the blue points in Fig. 6. These points and their corresponding heights were used to construct the BA curve.

The point distribution function was then constructed by counting the projected points that intersected the mesh within each step along the analysis direction. The point distribution function for strut 1 shown in Fig. 6 can be seen in the left image of Fig. 7. The bearing area curve was then calculated by integrating the point distribution function and normalizing the result by the total number of points. This then provides a function of the height at which a percentage of the total surface area



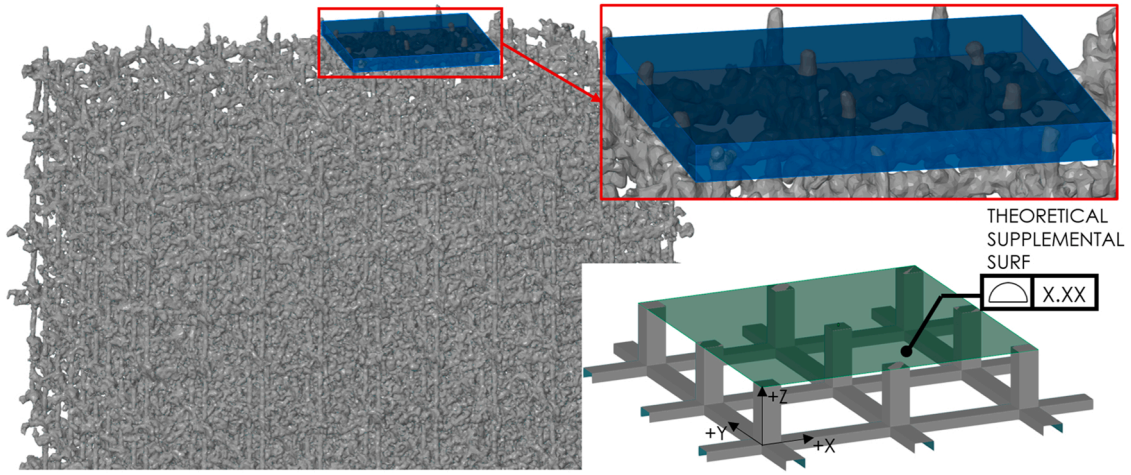


Fig. 4. Region of lattice structure and definition of form measurement.

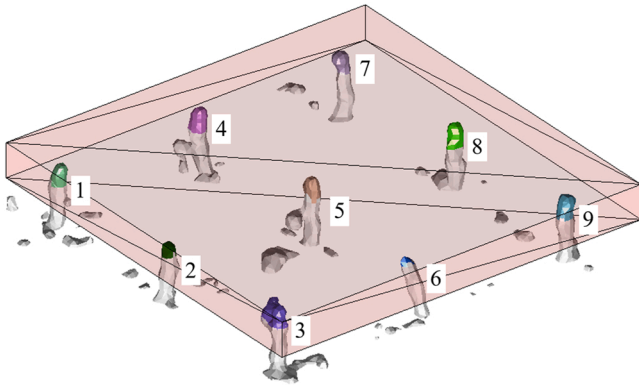


Fig. 5. Image of investigated struts. The investigation volume is shown as the transparent rectangular cuboid and individually segmented struts shown in unique mesh color and labeled.

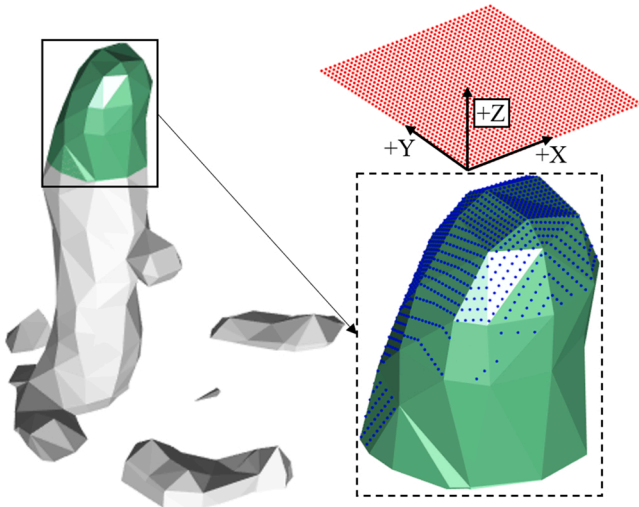


Fig. 6. Strut number 1 with the segmented area shown in green. The mesh discretization process is shown with the array of points shown in red and the points projected along the -Z direction are shown in blue on the surface.

was captured. The resulting bearing area curve can be seen in the right image of Fig. 7.

The partition point was then determined using the bearing area

curve. However, the methodology implemented in this work differed from that presented in Ref [25]. Because of the variations in strut geometry that can result from the AM process, wide variations in the bearing area curve shape are expected between different struts. Thus, a single partition point calculation methodology may not be suitable for all struts. In this work, three different partition point calculations were utilized.

The first partitioning methodology was identical to the process implemented in Ref [25]. The maximum point on the point distribution function was first identified. The point on the BA curve at the corresponding height was then identified, and two adjacent points in both the positive and negative directions along the BA curve were captured. A line was then fit to these five points via least-squares on the BA curve and was notated the “Peak Line”, referring to the peak in the point distribution function. A second line was then fit via least-squares to all data between a cumulative area of 90 % and 100 % on the bearing area curve and was defined as the “End Line”, signifying a sharp drop-off in the surface. The intersection of these two lines was defined as the partition point, which defines the transition point between the interior and exterior of the lattice. This methodology will be referred to as the “90–100” partitioning method.

The variations in BA curve shape resulting from form variations may necessitate a change in the partitioning methodology. For instance, if steep drop-offs in material are observed prior to the 90–100 region, this would indicate a height range in which little material is encountered followed by additional material. It could then be assumed that only the region prior to this steep drop-off should be utilized in the form calculation and that the material after the drop-off represents a secondary surface that should not be utilized in the form calculation. This change in assumptions is implemented in the second partitioning methodology, referred to as the “slope-based” partitioning method. Some initial operations were first performed on the BA curve to determine which partitioning method was appropriate for the given BA curve.

In the second partitioning methodology, the threshold slope was calculated for the given BA curve by determining the slope for a linear increase in material throughout the evaluation limits. Practically, this was completed by dividing the range of the evaluation limit by 100 %. The bearing area curve was then differentiated with respect to the cumulated area percentage. This curve was then examined to determine if there were three consecutive data points between cumulative areas of 10 % and 90 % that had values greater than the threshold slope previously determined. If yes, the slope-based partitioning was utilized. If multiple segments of the differentiated BA curve contained three or more consecutive values that were greater than the threshold slope, the segment occurring in the lowest area of cumulative area percentage was used. The End Line was then fit to these points. The Peak Line was then

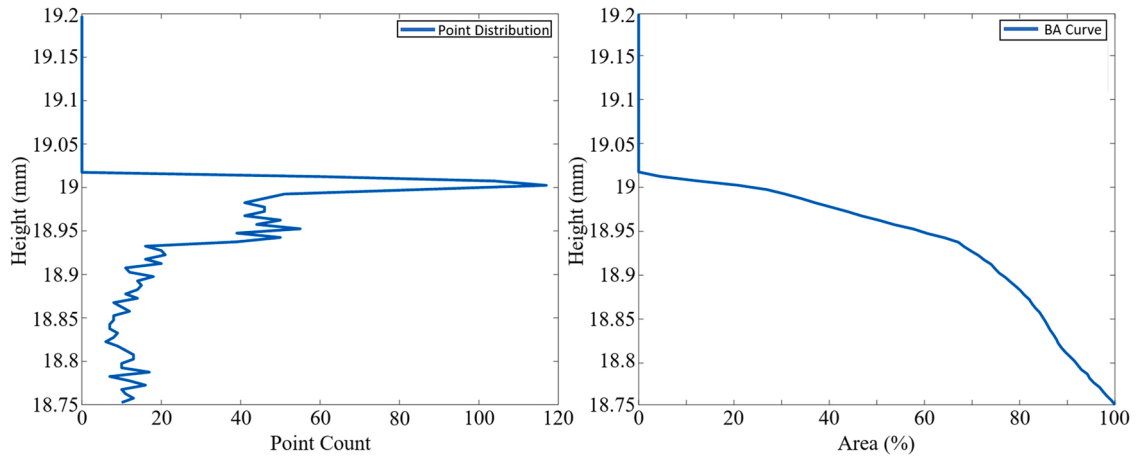


Fig. 7. Point distribution function and bearing area curve for strut 1.

fit similar to the 90–100 method, with one exception. The maximum value on the point distribution function was determined from the region of lower area percentage prior to the data utilized to fit the end line. This ensured that only surface data acquired prior to the end line, and thus “higher” on the surface, were used for the partition calculation. The intersection of these two lines was again determined to be the partition point.

In the calculation of the bearing area curve, it is also possible that no significant slope is observed. This is most likely to occur on lattice struts that were built shorter than intended. While the tops of these components will lie within the evaluation range, they may not be tall enough for a significant drop-off in data to be captured. While the evaluation range could be extended to fully capture this drop off, it will only lead to an unnecessary increase in the overall form of the inspected surface, as form is the measurement of the difference between the maximum deviations in opposite directions orthogonal to a fit feature. In this work, if no significant changes in the slope of the BA curve are found, the partition point was determined to be a cumulative area of 50 %. This is

referred to as the “50 %” method. Fig. 8 graphically displays the flow of data in the methodology implemented in this work.

As previously described, a nine strut portion of a lattice structure was investigated to examine the use of the three different partitioning methods. The struts were separated and were each investigated using BA partitioning. The values used in the methodology were set to 0.005 mm for both  $w$  and  $d$ . The extracted data from each strut was then used to assess the defined TSS. A plane was fit to this data using two different methods for comparison, least-squares and Chebyshev. This was done to highlight the influence of different fitting strategies on measurement results in the inspection of AM components. The BA curve calculations of select struts from the nine are presented in the following section, along with the final form measurement of the component using the two different fitting (association) methods.

#### 4. Results

Fig. 9(a) displays strut 5 from the lattice inspection set, and highlights the specific portion of the strut within the evaluation area from which the BA curve was constructed. The BA curve for this strut can be seen in Fig. 9(b). Several distinct regions are observable within this curve. The strut is first reached by the evaluation window at a height of 19.07 mm. The initial material peak is first encountered, displaying one

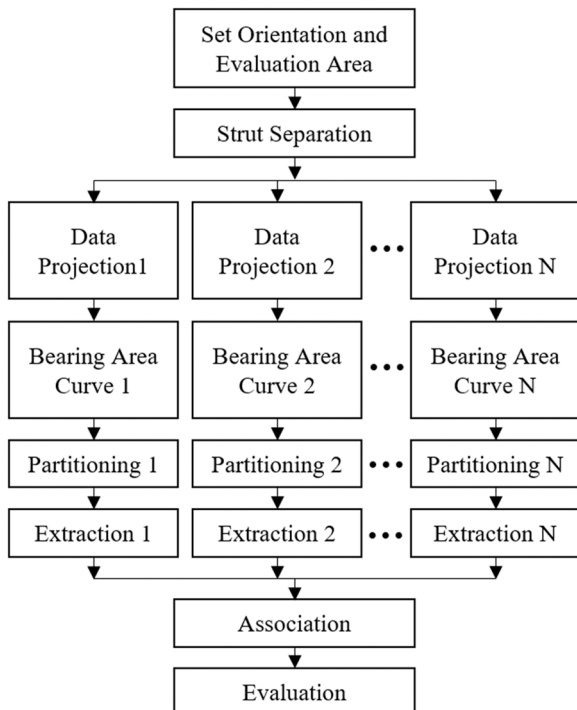


Fig. 8. Graphical depiction of the of the BA partitioning method.

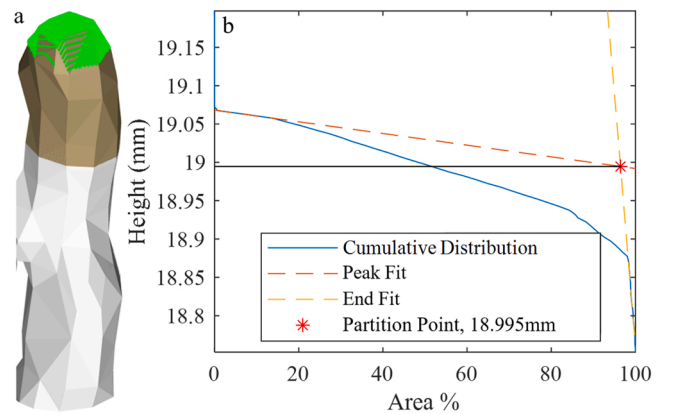
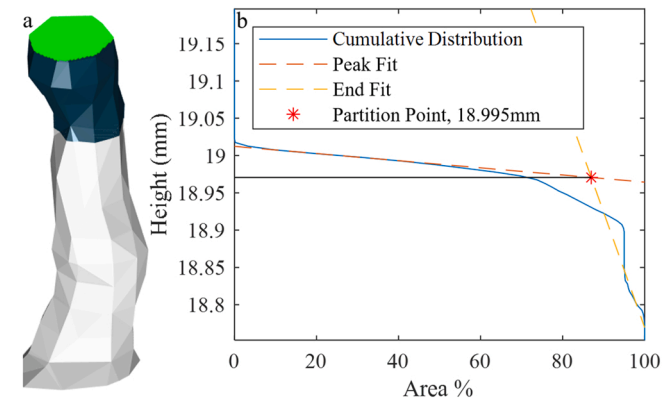


Fig. 9. (a) Strut number 5. The surface area within the investigation area has been shaded differently than the remainder of the strut while the extracted data points are shown in green. (b) The bearing area curve for strut number 5 and partition point determined by the 90–100 method. The beginning of the BA curve corresponds to the top of the lattice strut. The partition point corresponds to the lowest portion of the green extracted data and the end of the evaluation area (100 % on the BA curve) is the transition in shading on the strut.

distinct linear region. After this, a second linear region is observed, which extends from approximately 20–85 % of the BA curve. The slope of the BA curve then decreases more so after 85 % of the cumulative material, indicating another distinct region with lower surface area per unit height. Finally, the height data sharply drops off linearly at  $\approx 18.875$  mm, indicating a near vertical region on the component. While the region between 85 % and 99 % of the cumulative area does depict a distinctly sloped region, it is still below the threshold slope for the BA curve. The end of the evaluation area (100 % on the BA curve) can be observed on the strut as the transition between evaluated area (shown as the brown surface patches on the strut) and the remainder of the strut (shown as the grey surface patches). The steepest area of the BA curve occurs in the last  $\approx 1$  %, making 90–100 method preferential for this BA curve. The fit end line to the 90–100 % region is heavily skewed by the data below 18.875 mm, leading to a nearly vertical slope. The partition point was calculated to be 18.995 mm. Fig. 9(a) displays that strut 5 is largely vertical with a hemispherical top surface. The extracted data (shown as the green points in Fig. 9(a)) appears only on this hemispherical top surface and extends to slightly above the equator, indicating that the partitioning algorithm is performing as intended to capture the nominally flat top surface of the strut and capturing form deviations on this surface.

The results from the strut number 7 calculations are shown in Fig. 10. Slight differences in the BA curve can be observed between strut 5 and 7. The BA curve of strut 7 is shown to have a relatively flat top, signified by the substantial increase in cumulative area between 19.02 mm and 18.97 mm. This is then followed by a second sloped region between 75 % and 95 %. However, like strut 5, strut 7 is overall vertical, leading to a drop-off in the 95–100 % range. This, once again, shows good application of the 90–100 method. The slope of peak fit for both struts are fairly close to one another, indicating similar area capture in this area. However, the end fit for the two struts is very different, due to the more gradual drop in the 90–100 region. The partition point for strut 7 was calculated to be 18.971 mm.

The results from the BA partitioning of strut 4 show very different characteristics. In Fig. 11, three distinct regions can be observed in the BA curve. First, a linear region is observed between 0 % and 55 % showing a steady increase in area captured through the progression of the evaluation window. This is then followed by a transitional region in which the amount of area captured for each step of the evaluation window decreases. Finally, the BA curve once again becomes relatively linear until 100 % of the area is captured. The physical reason for this continual, gradual increase in material can be observed in Fig. 11 (a).



**Fig. 10.** (a) Strut number 7. The surface area within the investigation area has been shaded differently than the remainder of the strut while the extracted data points are shown in green. (b) The bearing area curve for strut number 7 and partition point determined by the 90–100 method. The beginning of the BA curve corresponds to the top of the lattice strut. The partition point corresponds to the lowest portion of the green extracted data and the end of the evaluation area (100 % on the BA curve) is the transition in shading on the strut.

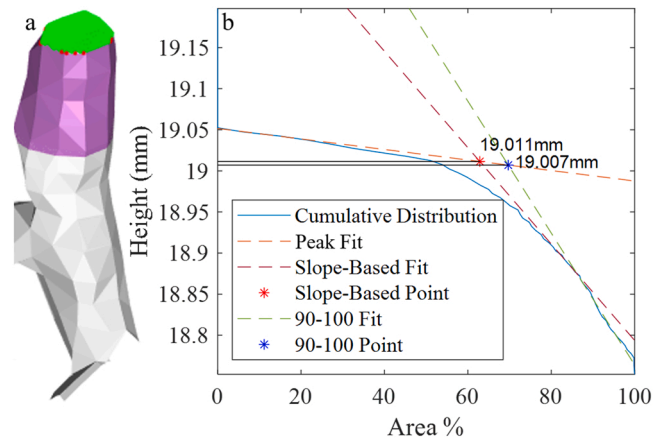


**Fig. 11.** (a) Strut number 4. The surface area within the investigation area has been shaded differently than the remainder of the strut while the extracted data points are shown in green and red for the 90–100 method. (b) The bearing area curve for strut number 4 and partition point determined by the slope-based method and the 90–100 method. The beginning of the BA curve corresponds to the top of the lattice strut. The partition points correspond to the lowest portion of the green extracted data and the end of the evaluation area (100 % on the BA curve) is the transition in shading on the strut.

The top of the strut is shown again to be semi-hemispherical, but the sides of the strut do not appear straight like strut 5. Instead, strut 4 appears almost conical, tapering wider from top to bottom within the evaluation area. A portion of this end linear region also has a slope greater than the threshold limit, therefore triggering the use of the slope-based method. In Fig. 10 (b), the results of the slope-based method and the 90–100 method are presented to contrast the results of both methods. In the slope-based method, the end line is fit to a cluster of points centralized around 84 % of the cumulative area. This method shifts the intersection of the end and peak lines to a lower cumulative area, and therefore higher point on the component, as opposed to fitting the end line to the 90–100 region. This more conservatively samples the surface compared to the partition point of 19.007 mm found using the 90–100 method, limiting data that extends onto the side of the strut, yielding a partition point of 19.011 mm.

The results from the strut 8 BA partitioning further exemplify the need for the slope-based method. In Fig. 11, the evaluation of strut 8 using both the slope-based and 90–100 methods is presented. One can see two distinct linear regions on the BA curve prior to 75 % cumulative area. This is followed by a sharp linear drop in the curve, indicating a near vertical region of surface area on the strut itself. This is then followed by another nominally linear region where more material is encountered per step of the evaluation window. In totality, this BA curve indicates an almost “stepped” surface, showing two distinct regions of surface area. This can be observed in Figs 12 and 13 (a), as there is an additional surface that extends out of the otherwise cylindrical strut. Thinking in context of geometry control on the top surface, only the initially contacted surface should be factored into the evaluation, as the side walls of the strut are not controlled geometry. Thus, if the slope-based method is used, the end line is fit to the drop-off between these two regions and calculated partition point for strut 8 is 18.982 mm. Ignoring this drop off and using the 90–100 method results in a partition point of 19.007 mm, shown as the red data in Fig. 11 (a). This results in an under-sampling of the surface due to the naïve fitting of the end line.

Strut number 6 displays a BA curve unlike the others observed in this data set. This strut is the lowest in the evaluation area of the struts inspected, resulting in a BA curve that doesn’t capture any component area until a height of 18.85 mm. This BA curve only shows one distinct linear region, which extends the entirety of the cumulative area. This indicates that only the top of the strut was investigated by the evaluation window, and that it did not extend onto the side surface of the struts.



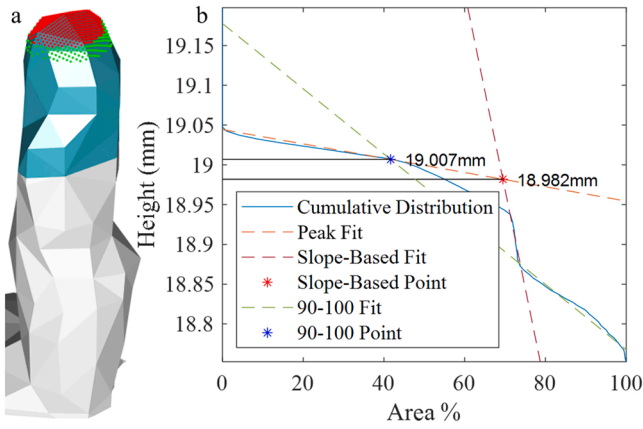


**Fig. 12.** (a) Strut number 8. The surface area within the investigation area has been shaded differently than the remainder of the strut while the extracted data points are shown in green for the sloped-based method and red for the 90–100 method. (b) The bearing area curve for strut number 8 and partition point determined by the slope-based method and the 90–100 method. The beginning of the BA curve corresponds to the top of the lattice strut. The partition points correspond to the lowest portion of the extracted data and the end of the evaluation area (100 % on the BA curve) is the transition in shading on the strut.

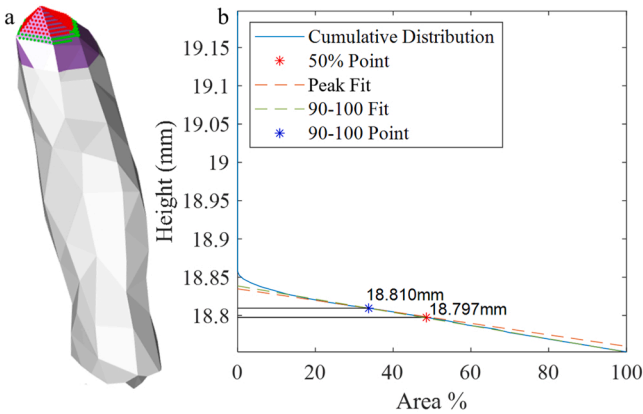


**Fig. 13.** (a) Strut number 6. The surface area within the investigation area has been shaded differently than the remainder of the strut while the extracted data points are shown in green for the sloped-based method and red for the 90–100 method. (b) The bearing area curve for strut number 6 and partition point determined by the 50 % method and the 90–100 method. The beginning of the BA curve corresponds to the top of the lattice strut. The partition points correspond to the lowest portion of the extracted data and the end of the evaluation area (100 % on the BA curve) is the transition in shading on the strut.

Thus, one could argue that the evaluation window should be extended further to capture these surfaces. However, since this strut is the lowest in the evaluation zone, extending the zone further down will likely only increase the extent of data sampled on the lattice, thereby increasing the magnitude of the form measurement. This may unnecessarily inflate the measurement, and cause the component to be determined out of specification. Extending the evaluation zone is also only viable up to a certain value, as eventually the evaluation window will contact the horizontal struts of the lattice. This option is not viable, as these surfaces are not defined by the theoretical supplemental surface. Thus, for the lowest lying strut in the evaluation area, the use of a different partitioning method may be appropriate. One could also argue that, for the measurement of form, the value will only be inflated further by the measurement of the lowest strut. Thus, only the top point of the lowest lying strut (provided that this point lies below all other partition points)

should be considered in the calculation of form. This should be further investigated in the calibration of this methodology using calibrated reference lattice structure. For this work, this strut was segmented using the 50 % method, as the partition point was determined to be the height at which 50 % of the cumulative area was captured, 18.797 mm. The 90–100 method was also utilized on this strut, indicating a partition point of 18.810 mm, indicating a decrease in the amount of data sampled.

The form of the component defined by the TSS was then determined using the BA segmented data from the five struts shown above and the remaining four struts. In one set, the algorithm was allowed to decide which partitioning method to use based on the criteria described above. For the second set, this decision was overridden to always use the 90–100 method. Figs 14 and 15 displays the results of these form measurements using the two different plane fitting algorithms, while Fig. 14 displays the form measurements using only the 90–100 method. Differences between the results of the two different plane fitting methods can be observed. The least-squares plane fitting leads to a higher form error than the Chebyshev plane fitting by 0.017 mm. While the difference between the two is only  $\approx 7\%$  of the total measurement, a significant difference in the fit feature can be seen in Fig. 14. The position of the fit feature on struts 7 and 9 (using the notation from Fig. 5) is observably lower in the Chebyshev fitting. However, by nature of the least-squares method, the average deviation from the fit feature is minimized. Each of these methods will be affected by the results from the individual BA curve partitioning calculations on the individual struts. The least-squares fitting algorithm will be weighted more by struts that have a larger number of points, thus skewing the fit plane towards struts with larger surface area. The Chebyshev fitting algorithm will be heavily influenced by the partitioning of the shortest strut, as it is heavily influenced by outlier points. Furthermore, the calculation of form, in this case flatness, is by definition the orthogonal distance between maximum and minimum points. Thus, the partitioning of the lowest strut will have an immediate effect on the minimum deviation (highest negative variation) and therefore the overall measured flatness. For these components, it may be pertinent to analyze other characteristics of the defined surfaces, as the distribution of form variation may be a more useful metric than the overall maximum variation.

Fig. 14 displays the fitting results of the lattice partitioning based on the criteria above to only using the 90–100 method. In the Chebyshev fit feature, the measurement of form has decreased from 0.243 mm to 0.239 mm. This agrees with the results observed in Fig. 12, where the partition point was moved higher using the 90–100 method. Since the highest point on the lattice remains unchanged, the min-max zone of the material would decrease if the partition point was raised. However, the measurement of form has increased in the least-squares fit feature. This is likely due to changes in the partition of the struts skewing the orientation of the fit feature for form assessment. On strut 3, a large amount of data is included in the calculation of form using the least-squares fit feature. A dense cluster of points on a single strut will unevenly weight the least-squares fitting toward the individual strut, thus changing the orientation of the plane from which flatness is measured. This then leads to a change in the normal along which the measurement is calculated and increases the measured value.

The integration of the slope-based partitioning methodology into the measurement of form on a lattice structure has been demonstrated here as an intelligent alternative to the 90–100 method. The presented results indicate appropriate partitioning of lattice struts of varying geometry acquired from XCT measurements of an AM lattice structure. However, it is difficult to definitively say which of these partitioning methods is the most accurate, as there is no reference value to compare the measurement results against. Future work will focus on the calibration of this methodology using well defined reference lattice structures.



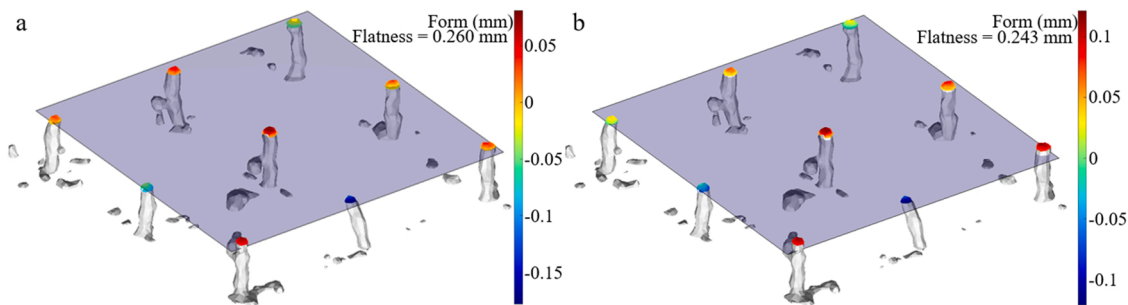


**Fig. 14.** Final form measurements using two different plane fitting algorithms on the extracted data. The fit plane is shown transparent while the normal deviation from the fit plane is shown for each point on the color scale to the left of the figure. (a) Least-squares [Gaussian] (b) Chebyshev [min-max].

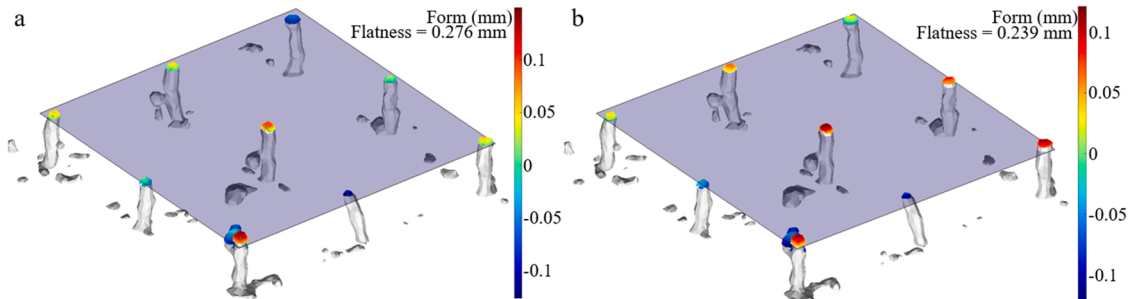


**Fig. 15.** Final form measurements using two different plane fitting algorithms on the extracted data using only the 90–100 method. The fit plane is shown transparent while the normal deviation from the fit plane is shown for each point on the color scale to the left of the figure. (a) Least-squares [Gaussian] (b) Chebyshev [min-max].

## 5. Conclusion

In this work, the BA partitioning methodology was implemented on data obtained through XCT measurements of an AM lattice structure. A BA partitioning methodology was adapted to segment the struts of the lattice structure and determine form variations resulting from the manufacturing process. This newly presented BA partitioning method utilizes three different criteria to calculate the partition point, based on features of the calculated BA curve for a given lattice strut: 90–100, slope-based, and 50 %. The individual partition point calculations appear highly applicable to the form variations seen from AM components and the methodology is able to adapt to different BA curve forms. Using the three-criteria partitioning approach is shown to improve the flexibility of the methodology as compared to only using the 90–100 method. The influence of the plane fitting algorithm on the measurement result is also shown to have an effect on the measurement result. Differences in orientation and location of the fit feature are observed and are likely to be influenced by the partition point calculation. This could have significant impact on the alignment of the component if TSS surfaces are used as datums and is applicable to external surfaces oriented in any direction. Future work will focus on the assessment of accuracy and repeatability of the BA partitioning method by utilizing calibrated AM lattice structures. These works will include surface partitioning and height calculation. Additional metrics will also be investigated to evaluate the form of the lattice, such as analysis on the distribution of form variations compared to the TSS. This methodology is also likely transferable to other geometries besides planes, such as cylindrical or spherical surfaces, via a transformation of coordinates and translation along the radial direction. The use of this BA partitioning methodology will be investigated on these non-planar surfaces in future work.

## CRediT authorship contribution statement

**Maxwell Praniewicz:** Conceptualization, Methodology, Software, Formal Analysis, Investigation, Writing – Original Draft. **Lucas Fournet-**

**Fayard:** Methodology, Resources, Investigation, Writing – Review & Editing. **Jason Fox:** Conceptualization, Methodology, Writing – Review & Editing, Supervision. **Charles Cayron:** Resources, Review & Editing, Supervision. **Imade Koutiri:** Resources, Review & Editing, Supervision. **Anne-Françoise Obaton:** Resources, Review & Editing, Supervision.

## Declaration of Competing Interest

The authors declare that they have no known competing financial interests or personal relationships that could have appeared to influence the work reported in this paper.

## Data availability

Data will be made available on request.

## Acknowledgements

Work completed by NIST was performed through funding from the Measurement Science for Additive Manufacturing (MSAM) program. Work completed elsewhere was performed in the framework of the Additive Factory Hub (AFH) based in Saclay, France, which is a private platform financing academic research in the field of metal additive manufacturing. Carl Zeiss Services is thanked for the XCT scans and their help in the measurement protocol.

## References

- [1] ASTM International, "ISO/ASTM 52900:2021 Additive manufacturing - General principles - Terminology," West Conshohocken, PA, Nov. 2021.
- [2] A. Nazir, K.M. Abate, A. Kumar, J.-Y. Jeng, A state-of-the-art review on types, design, optimization, and additive manufacturing of cellular structures, *Int J. Adv. Manuf. Technol.* vol. 104 (9) (2019) 3489–3510, <https://doi.org/10.1007/s00170-019-04085-3>.
- [3] P. Zhang, J. Liu, A.C. To, Role of anisotropic properties on topology optimization of additive manufactured load bearing structures, *Scr. Mater.* vol. 135 (2017) 148–152, <https://doi.org/10.1016/j.scriptamat.2016.10.021>.

- [4] L.-Y. Chen, S.-X. Liang, Y. Liu, L.-C. Zhang, Additive manufacturing of metallic lattice structures: Unconstrained design, accurate fabrication, fascinated performances, and challenges, *Mater. Sci. Eng.: R. Rep.* vol. 146 (2021), 100648, <https://doi.org/10.1016/j.mser.2021.100648>.
- [5] A. Thompson, I. Maskery, R.K. Leach, X-ray computed tomography for additive manufacturing: a review, *Art. no. 7, Meas. Sci. Technol.* vol. 27 (7) (2016).
- [6] B. Lozanovski, et al., Non-destructive simulation of node defects in additively manufactured lattice structures, *Addit. Manuf.* vol. 36 (2020), 101593, <https://doi.org/10.1016/j.addma.2020.101593>.
- [7] M. Dallago, B. Winiarski, F. Zanini, S. Carmignato, M. Benedetti, On the effect of geometrical imperfections and defects on the fatigue strength of cellular lattice structures additively manufactured via Selective Laser Melting, *Int. J. Fatigue* vol. 124 (2019) 348–360, <https://doi.org/10.1016/j.ijfatigue.2019.03.019>.
- [8] I. Echeta, B. Dutton, R.K. Leach, S. Piano, Finite element modelling of defects in additively manufactured strut-based lattice structures, *Addit. Manuf.* vol. 47 (2021), 102301, <https://doi.org/10.1016/j.addma.2021.102301>.
- [9] Z. Chen, C. Han, M. Gao, S.Y. Kandukuri, K. Zhou, A review on qualification and certification for metal additive manufacturing, *Virtual Phys. Prototyp.* vol. 17 (2) (2022) 382–405, <https://doi.org/10.1080/17452759.2021.2018938>.
- [10] R.K. Leach, D. Bourell, S. Carmignato, A. Donmez, N. Senin, W. Dewulf, Geometrical metrology for metal additive manufacturing, *CIRP Ann.* vol. 68 (2) (2019) 677–700, <https://doi.org/10.1016/j.cirp.2019.05.004>.
- [11] W. Dewulf, H. Bosse, S. Carmignato, R. Leach, Advances in the metrological traceability and performance of X-ray computed tomography, *CIRP Ann.* vol. 71 (2) (2022) 693–716, <https://doi.org/10.1016/j.cirp.2022.05.001>.
- [12] A. du Plessis, G. Schwaderer, I. Cristofolini, M. Zago, M. Benedetti, Dimensional metrology of additively manufactured lattice structures by combined tactile probe and X-ray tomography, *Mater. Des. Process. Commun.* (2020), <https://doi.org/10.1002/mdp2.216>.
- [13] F. Zanini, M. Sorgato, E. Savio, S. Carmignato, Dimensional verification of metal additively manufactured lattice structures by X-ray computed tomography: use of a newly developed calibrated artefact to achieve metrological traceability, *Addit. Manuf.* (2021), 102229, <https://doi.org/10.1016/j.addma.2021.102229>.
- [14] M. Pranievicz, J.C. Fox, C. Saldana, Toward traceable XCT measurement of AM lattice structures: Uncertainty in calibrated reference object measurement, *Precis. Eng.* vol. 77 (2022) 194–204, <https://doi.org/10.1016/j.precisioneng.2022.05.010>.
- [15] Y. Amani, S. Dancette, P. Delroisse, A. Simar, E. Maire, Compression behavior of lattice structures produced by selective laser melting: X-ray tomography based experimental and finite element approaches, *Acta Mater.* vol. 159 (2018) 395–407, <https://doi.org/10.1016/j.actamat.2018.08.030>.
- [16] ASME, “ASME Y14.46–2022 Product Definition for Additive Manufacturing,” 2022.
- [17] G. Ameta, J. Fox, P. Witherell, Tolerancing and verification of additive manufactured lattice with supplemental surfaces, *Procedia CIRP* vol. 75 (2018) 69–74.
- [18] B.S. Rupal, N. Anwer, M. Secanell, A.J. Qureshi, Geometric tolerance and manufacturing assemblability estimation of metal additive manufacturing (AM) processes, *Mater. Des.* vol. 194 (2020), 108842, <https://doi.org/10.1016/j.matdes.2020.108842>.
- [19] M. Pranievicz, G. Ameta, J. Fox, C. Saldana, Data registration for multi-method qualification of additive manufactured components, *Addit. Manuf.* vol. 35 (2020), 101292, <https://doi.org/10.1016/j.addma.2020.101292>.
- [20] M. Pranievicz, J. Fox, G. Ameta, F. Kim, P. Witherell, C. Saldana, Exploring registration of optical, CMM and XCT for verification of supplemental surfaces to define AM lattices: application to cylindrical and spherical surfaces, *Procedia CIRP* vol. 92 (2020) 181–186, <https://doi.org/10.1016/j.procir.2020.05.182>.
- [21] International Organization for Standardization, “ISO 17450–1:2011 Geometrical product specifications (GPS) - General concepts - Part 1: Model for geometrical specification and verification,” International Organization for Standardization, 2011.
- [22] E.J. Abbott, F.A. Firestone, Specifying surface quality: a method based on accurate measurement and comparison, *Mech. Eng.* vol. 55 (9) (1933) 569–572.
- [23] S. Lou, Z. Zhu, W. Zeng, C. Majewski, P.J. Scott, X. Jiang, Material ratio curve of 3D surface topography of additively manufactured parts: an attempt to characterise open surface pores, *Surf. Topogr.: Metrol. Prop.* vol. 9 (1) (2021), 015029, <https://doi.org/10.1088/2051-672X/abedf9>.
- [24] A. Molinari, et al., Effect of process parameters on the surface microgeometry of a Ti6Al4V alloy manufactured by laser powder bed fusion: 3D vs. 2D characterization, *Art. no. 1, Metals* vol. 12 (1) (2022), <https://doi.org/10.3390/met12010106>.
- [25] M. Pranievicz, J.C. Fox, C. Saldana, An investigation into the definition and qualification of form of lattice structures, *JOM* (2021), <https://doi.org/10.1007/s11837-021-05030-0>.